AGU PUBLICATIONS

JGR

Journal of Geophysical Research: Space Physics

RESEARCH ARTICLE
10.1002/2015JA021592

Giant pulsations on the afternoonside: Geostationary satellite and ground observations

Tetsuo Motoba[1,2], Kazue Takahashi[1], Juan V. Rodriguez[3,4], and Christopher T. Russell[5]

[1]The Johns Hopkins University Applied Physics Laboratory, Laurel, Maryland, USA, [2]Now at Solar-Terrestrial Environment Laboratory, Nagoya University, Nagoya, Japan, [3]Cooperative Institute for Research in Environmental Sciences, University of Colorado Boulder, Boulder, Colorado, USA, [4]National Centers for Environmental Information, National Oceanic and Atmospheric Administration, Boulder, Colorado, USA, [5]Institute of Geophysics and Planetary Physics, University of California, Los Angeles, California, USA

Key Points:
- Statistical survey of giant pulsations in 2008-2013
- Coordinated GOES-ground observations of giant pulsations
- Wave-particle interactions with giant pulsations

Correspondence to:
T. Motoba,
tetsuo.motoba@gmail.com

Citation:
Motoba, T., K. Takahashi, J. V. Rodriguez, and C. T. Russell (2015), Giant pulsations on the afternoonside: Geostationary satellite and ground observations, *J. Geophys. Res. Space Physics*, *120*, 8350–8367, doi:10.1002/2015JA021592.

Received 19 JUN 2015
Accepted 27 AUG 2015
Accepted article online 3 SEP 2015
Published online 5 OCT 2015

Abstract Giant pulsations (Pgs) are a special class of oscillations recognized in ground magnetometer records as exhibiting highly regular sinusoidal waveforms in the east-west component with periods around 100s. Previous statistical studies showed that Pgs occur almost exclusively on the morningside with peak occurrence in the postmidnight sector. In this paper, we present observations of Pgs extending to the afternoonside, using data from the GOES13 and 15 geostationary satellites and multiple ground magnetometers located in North America. For a long-lasting event on 29 February 2012, which spanned ~08–18h magnetic local time, we show that basic Pg properties did not change with the local time, although the period of the pulsations was longer at later local time due to increasing mass loading. There is evidence that the Pgs resulted from fundamental poloidal mode standing Alfvén waves, both on the morning and afternoonsides. Oscillations of energetic particles associated with the field oscillations exhibited an energy-dependent phase, which has previously been reported and explained by drift resonance. A statistical analysis of the ground magnetic field data ($L = 3.8–7.4$) covering 2008–2013 confirms that afternoon Pgs are not unusual. We identified a total of 105 Pg events (about 70% (30%) of the events occurred during non-storm (late storm recovery) periods), 31 of which occurred on the afternoonside. The afternoon Pgs occur under solar wind and geomagnetic conditions that are similar to the morning Pgs, but the afternoon Pgs tend to have short durations and occur frequently in winter instead of around spring and fall equinoxes that are favored by the morning Pgs.

1. Introduction

Giant pulsations (Pgs) are a special class of ultralow-frequency (ULF) waves observed on the ground most often at auroral latitudes [*Birkeland*, 1901] with periods usually around 100s but at times as short as 60s or as long as 200s [*Brekke et al.*, 1987, and references therein]. Pgs are characterized by a highly sinusoidal waveform, a strong magnetic field perturbation in the east-west direction, strong latitudinal localization, westward propagation, and an azimuthal wave number (m) in the range of 16–35 [*Takahashi et al.*, 1992, and references therein]. Pgs are rare [e.g., *Brekke et al.*, 1987], and because ground-satellite conjunction is essential in the search for the magnetospheric source wave for Pgs, ground-satellite studies of Pgs have heavily relied on geostationary satellites. Unfortunately, geostationary satellites usually carry limited scientific experiments, and as a result, the mode structure and source mechanism of Pgs had remained inconclusive [*Kokubun*, 1980; *Glassmeier et al.*, 1999; *Thompson and Kivelson*, 2001].

Recent studies using well-instrumented satellites on low-inclination elliptical orbits significantly advanced our understanding of Pgs. First, ground-satellite study of an event using a Time History of Events and Macroscale Interactions during Substorms (THEMIS) spacecraft and multiple ground magnetometers provided convincing evidence that Pgs originate from fundamental standing Alfvén waves with a strong poloidal component [*Takahashi et al.*, 2011]. In addition, a study using the Van Allen Probes [*Dai et al.*, 2013] provided evidence that an earthward gradient of the phase space density of ring current ions feeds energy to fundamental poloidal mode waves through drift resonance [e.g., *Southwood*, 1976; *Chen and Hasegawa*, 1991], although the Dai et al. study did not report that the wave observed in space produced Pgs on the ground.

An outstanding and unexplained feature of Pgs is that they occur most often during years of minimum solar activity and almost exclusively on the morningside [*Brekke et al.*, 1987; *Chisham and Orr*, 1991]. A model

©2015. American Geophysical Union. All Rights Reserved.

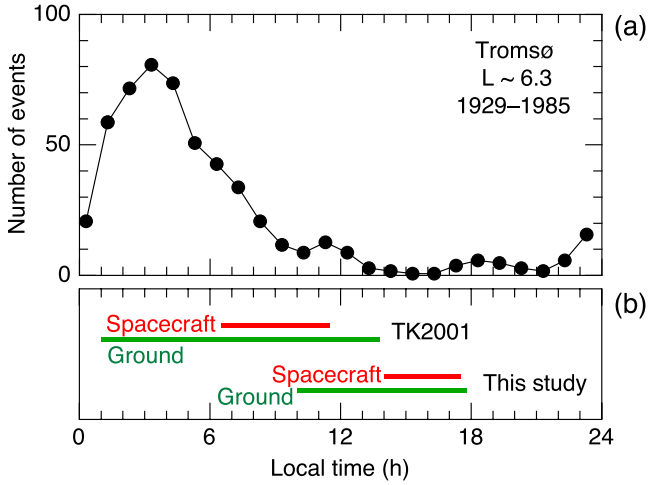

Figure 1. (a) Local time distribution of Pgs observed at Tromsø (L~6.3) [*Brekke et al.*, 1987]. (b) Local time span of a Pg event observed with a geostationary satellite and ground magnetometers [*Thompson and Kivelson*, 2001, TK2001] and a Pg event observed with geostationary satellites and ground magnetometers that is included in the present study.

particle orbit study [*Chisham*, 1996] indicated that the spatial occurrence pattern of Pgs can be explained by the drift path of protons with energies ~5–30keV, if the pulsations are excited by bounce resonance of the protons with second harmonic standing waves. Although we cannot exclude the possibility that some Pgs have a second harmonic standing wave structure, ground-satellite conjugate observations overwhelmingly favor a fundamental standing wave structure for Pgs [*Kokubun*, 1980; *Hillebrand et al.*, 1982; *Kokubun et al.*, 1989; *Takahashi et al.*, 1992; *Thompson and Kivelson*, 2001; *Takahashi et al.*, 2011]. Obviously, the *Chisham* model does not apply to fundamental standing waves. Fundamental standing waves are possibly excited by drift resonance of protons with energy around 100keV [*Thompson and Kivelson*, 2001; *Dai et al.*, 2013], but no drift path calculation of these protons has been conducted to explain the spatial occurrence pattern of Pgs. It is unclear whether other generation mechanisms of fundamental standing waves such as drift wave instability [*Green*, 1979] can explain the localization of Pgs in local time (LT). No theoretical study has explained why the occurrence of Pgs depends on solar activity.

In this paper, we report the LT dependence of Pg activity during 2008–2013, which covers the first half of solar cycle 24. This work was intended to be a preliminary event survey for a satellite-ground correlative study of the Pg source mechanism using observations with the THEMIS spacecraft, launched in 2007, and the Van Allen Probes, launched in 2012. To our surprise, we found that the local time distribution of Pgs differs significantly from those reported previously. Therefore, in this paper we report the local time dependence of Pg occurrence as a stand-alone piece of work, using observations on the ground and at the GOES geostationary satellites.

To put our study into a historical perspective, we show in Figure 1a the LT distribution of Pgs reported by *Brekke et al.* [1987]. The distribution was obtained by examining magnetic field variations that were photographically recorded at Tromsø, Norway (geographic latitude 69.7°, geographic longitude 18.9°, L~6.3), from 1929 to 1985. Note that we have changed the horizontal axis from universal time (UT) in the original figure to LT using the relationship LT = UT + 1.3h. Pg events are concentrated in the 00–06h LT sector, and the occurrence is very low from 13 to 22h LT. The upper pair of horizontal bars shown in Figure 1b indicates the local time span of a long-lasting Pg event observed both on the ground (green line) and at a geosynchronous spacecraft (red line) [*Thompson and Kivelson*, 2001]. The lower pair indicates the local time span of a Pg event on 29 February 2012, which is reported in the present study. It is evident that the local time extent of our event is unique.

The remainder of the paper is organized as follows. Section 2 describes the experiments and data. Section 3 presents a detailed examination of the event on 29 February 2012. Section 4 describes statistical analyses of Pgs observed on the ground. Section 5 presents the discussion, and section 6 concludes the study.

2. Experiments and Data

This study uses data acquired by the GOES13 and GOES15 geostationary satellites and by ground magnetometers located in North America. The GOES data are used to study an event on 29 February 2012.

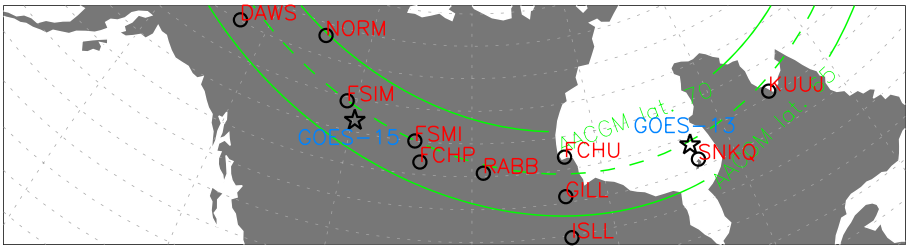

Figure 2. Map of ground magnetometer stations providing data for the 29 February 2012 Pg event. The stars indicate the magnetic field footprints of GOES13 and GOES15.

During this event, the satellites were located over North America at the geographic longitudes of 74.5° W (GOES13) and 135.8°W (GOES15). Figure 2 shows the magnetic field footprints of the satellites given by the Tsyganenko 1996 (T96) magnetic field model [*Tsyganenko*, 1995].

GOES data used in the present study are magnetic field vectors and energetic particle fluxes. The GOES digital data files as well as the associated documents are provided by NOAA (http://www.ngdc.noaa.gov/stp/satellite/goes/dataaccess.html). The magnetic field measurements were made with a three-axis fluxgate magnetometer (0.512s sampling resolution) [*Singer et al.*, 1996], which is part of the Space Environmental Monitoring (SEM) experiment. We have rotated the magnetic field vectors into a local magnetic field-aligned coordinate system that uses the T89c model field [*Tsyganenko*, 1989] as the reference [e.g., *Takahashi et al.*, 2010]. In this system, the three orthogonal axes are given by $\mathbf{e}_v$ (radially outward), $\mathbf{e}_\phi$ (eastward), and $\mathbf{e}_\mu$ (parallel to the model magnetic field).

The particle fluxes were measured by other experiments in the SEM suite: the Magnetospheric Proton Detector (MAGPD) and the Magnetospheric Electron Detector (MAGED). MAGPD and MAGED each consists of nine telescopes mounted on the anti-Earth side of the spacecraft with look directions at 0°, ±35°, and ±70° from the anti-Earth direction in both the equatorial and azimuthal planes. Each telescope has a full detection cone angle of 30°. MAGPD measures protons in five differential energy channels centered at 95, 140, 210, 300, and 575keV, while MAGED measures electrons in five differential energy channels centered at 40, 75, 150, 275, and 475keV. In this study, we use 1min averages of particle fluxes covering the pitch angle range of 75–105°.

We use ground magnetometer data to identify Pgs in both the case and statistical studies. In the case study of the 29 February 2012 Pg event, we use data from 11 stations selected from the THEMIS Ground-Based Observatories (GBO) [*Mende et al.*, 2008; *Russell et al.*, 2008], the Canadian Array for Realtime Investigations of

Table 1. Ground Magnetometers Used for the 29 February 2012 Pg Event

Station	Code	Geographic Latitude (deg)	Geographic Longitude (deg)	Magnetic Latitude (deg)	Magnetic Longitude (deg)	*L*
Kuujjuarapik[a]	KUUJ	58.10	291.60	66.70	14.25	6.39
Sanikiluaq[b]	SNKQ	56.50	280.80	66.81	356.67	6.45
Fort Churchill[c]	FCHU/FCC	58.76	265.92	68.32	333.54	7.44
Island Lake[c]	ISLL	53.86	265.34	63.62	333.36	5.15
Gillam[a,c]	GILL	56.38	265.36	66.03	333.05	6.15
Rabbit Lake[c]	RABB	58.22	256.32	66.85	319.11	6.57
Fort Smith[a,c]	FSMI	60.02	248.05	67.28	306.90	6.81
Fort Chipewyan[c]	FCHP	58.77	248.89	66.23	308.55	6.25
Fort Simpson[a,c]	FSIM	61.76	238.77	67.23	294.29	6.78
Norman Wells[c]	NORM	65.26	233.31	69.53	285.74	8.31
Dawson City[c]	DAWS	64.05	220.89	65.90	273.89	6.09

[a]THEMIS GBO/EPO
[b]CANMOS
[c]CARISMA

Table 2. Ground Magnetometers Used for Statistics

Station	Code	Geographic Latitude (deg)	Geographic Longitude (deg)	Magnetic Latitude (deg)	Magnetic Longitude (deg)	*L*
Kuujjuarapik[a]	KUUJ	58.10	291.60	66.70	14.25	6.39
Chibougamou[a]	CHBG	49.81	285.58	59.25	4.54	3.83
Sanikiluaq[a,b]	SNKQ	56.50	280.80	66.81	356.67	6.45
Kapuskasing[a]	KAPU	49.39	277.68	59.51	353.00	3.88
Fort Churchill[a,b,c]	FCHU/FCC	58.76	265.92	68.32	333.54	7.44
Gillam[a,c]	GILL	56.38	265.36	66.03	333.05	6.15
Pinawa[a,c]	PINA	50.20	263.96	59.96	332.57	3.99
Fort Smith[a,c]	FSMI	60.02	248.05	67.28	306.90	6.81
Fort Simpson[a,c]	FSIM	61.76	238.77	67.23	294.29	6.78
Gakona[d]	GAKO	62.39	214.87	63.40	270.15	4.99
Fort Yukon[d]	FYKN	66.56	214.79	67.65	267.26	6.92
Poker Flat[d]	POKR	65.12	212.57	65.79	266.38	5.95
College[d,e]	CIGO/CMO	64.87	212.14	65.45	266.18	5.79
Kiana[a]	KIAN	66.97	199.56	65.59	254.44	5.85

[a]THEMIS GBO/EPO
[b]CANMOS
[c]CARISMA
[d]University of Alaska
[e]USGS

Magnetic Activity (CARISMA) [*Mann et al.*, 2008], and the CANadian Magnetic Observatory System (CANMOS) arrays (http://geomag.nrcan.gc.ca/obs/canmos-eng.php). The stations are listed in Table 1, and their locations are shown in Figure 2.

In the statistical study, we use data archived in the Coordinated Data Analysis Web database from the following sources: THEMIS GBO, CARISMA, CANMOS, the Geophysical Institute Magnetometer Array (https://www.asf.alaska.edu/magnetometer/), and the U.S. Geological Survey (USGS; http://geomag.usgs.gov/). Table 2 provides the information on the magnetometers used in the statistical analysis.

The time resolution of the magnetometer data is 0.5s or 1.0s, with the exception of Sanikiluaq (SNKQ, 1min) used for the case study. The horizontal components of the magnetic field vector at the CARISMA and CANMOS arrays are expressed using the *X* (northward) and *Y* (eastward) components in geographic coordinates. For the other arrays, the horizontal components are expressed in *H-D* coordinates, where *H* is magnetically northward and *D* is eastward.

3. Pg Event on 29 February 2012

We first examine a Pg event that was observed on the afternoonside as well as on the morningside. The uniqueness of the event was already described briefly in section 1 using Figure 1. We show that despite the large local time extent, the event shares basic properties with typical morning Pgs.

3.1. Solar Wind Condition and Geomagnetic Activity

Figure 3 shows the solar wind 1min OMNI data (http://omniweb.gsfc.nasa.gov) for 29 February to 1 March 2012, together with the provisional geomagnetic indices (*AU*/*AL* and *Dst*) obtained from the World Data Center for Geomagnetism, Kyoto. The gray shading, covering 1800–2400 UT, indicates the time interval of simultaneous observation of the Pg event at GOES and at the ground magnetometer stations listed in Table 1.

The solar wind magnetic field was directed northward (Figure 3a), and no large variations are seen in the velocity (Figure 3b) from ~12h before until well after the Pg event. The dynamic pressure (Figure 3c) decreased by a factor of ~3 at the middle of the Pg activity, but this reduction cannot be the reason for Pg excitation because of the time delay from the Pg onset. Consistent with the northward interplanetary magnetic field (IMF), the geomagnetic activity was very low, as seen in both the *AL*/*AU* indices (Figure 3d) and *Dst* index

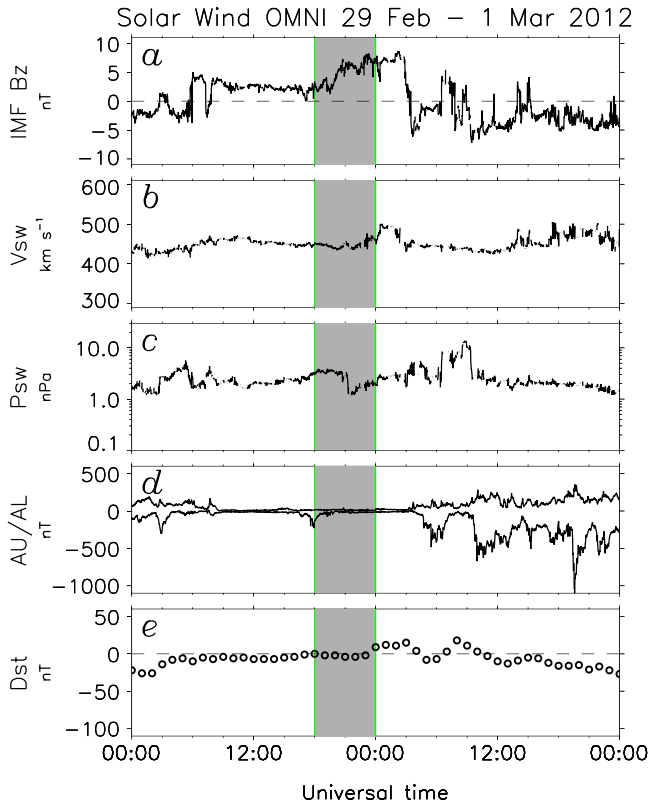

Figure 3. Solar wind parameters from the OMNI database for 29 February to 1 March 2012, along with geomagnetic indices. The shading highlights an interval of Pgs. (a) IMF *z* component in the geocentric solar magnetospheric coordinates. (b) Solar wind speed. (c) Solar wind dynamic pressure. (d) *AU*/*AL* index. (e) *Dst* index.

(Figure 3e). The only disturbance visible is a small *AL* minimum of −229 nT that occurred at 1756 UT, before the start of the Pg event. Pgs are known to occur during geomagnetically quiet periods [e.g., *Brekke et al.*, 1987], but a small substorm might be necessary to inject ions into the ring current for Pgs to be excited.

3.2. Local Time Extent of the Pg Event on the Ground

Figure 4 presents the magnetic field records from selected stations in Canada that form an east-west chain in the geomagnetic latitude range of 65°–70° (L = 6.1–8.4). See Table 1 and Figure 2 for the station locations. Figures 4 (left column) and 4 (right column) show the *X* (northward) and *Y* (eastward) components, respectively. The rows are ordered by the longitude of the stations, with the longitude changing progressively westward from top to bottom. The orange and blue vertical lines mark magnetic noon and midnight, respectively.

In the compressed time series plots of Figure 4, Pgs are recognized as slowly varying envelopes, which are more prominent in *Y* than in *X*. This envelope structure is most persistent at Rabbit Lake (RABB, L = 6.5). At this location, the envelope started to grow at ~1830 UT and lasted until ~2400 UT, with the width of the envelope reaching ~15nT at ~2000 UT and ~2300 UT. Traditionally, a Pg is defined to be a highly monochromatic oscillation with a strong perturbation in the east-west component, and our event meets this definition. We have confirmed the regular waveform at each station using plots with expanded time axes. A similar envelope structure is seen at a few other stations close to RABB: Gillam (GILL), Fort Chipewyan (FCHP), and Fort Smith (FSMI). To the east of these stations, an envelope structure with lesser prominence is seen, at Kuujjuarapik (KUUJ), SNKQ, and Fort Churchill (FCHU). To the east (at Fort Simpson (FSIM), Norman Wells (NORM), and Dawson City (DAWS)), however, such an envelope structure is absent.

Figure 5 summarizes the spectral contents and the local time span of the Pgs on the ground. Figure 5a shows the dynamic power spectra of the magnetic *Y* components for 1800–2400 UT at the 10 stations shown in Figure 4. The frequency of the Pgs is ~6mHz at all stations and changes little over time. Figure 5b tracks the UT and magnetic local time (MLT) of the Pgs at the ground stations (black) and the poloidal mode waves at

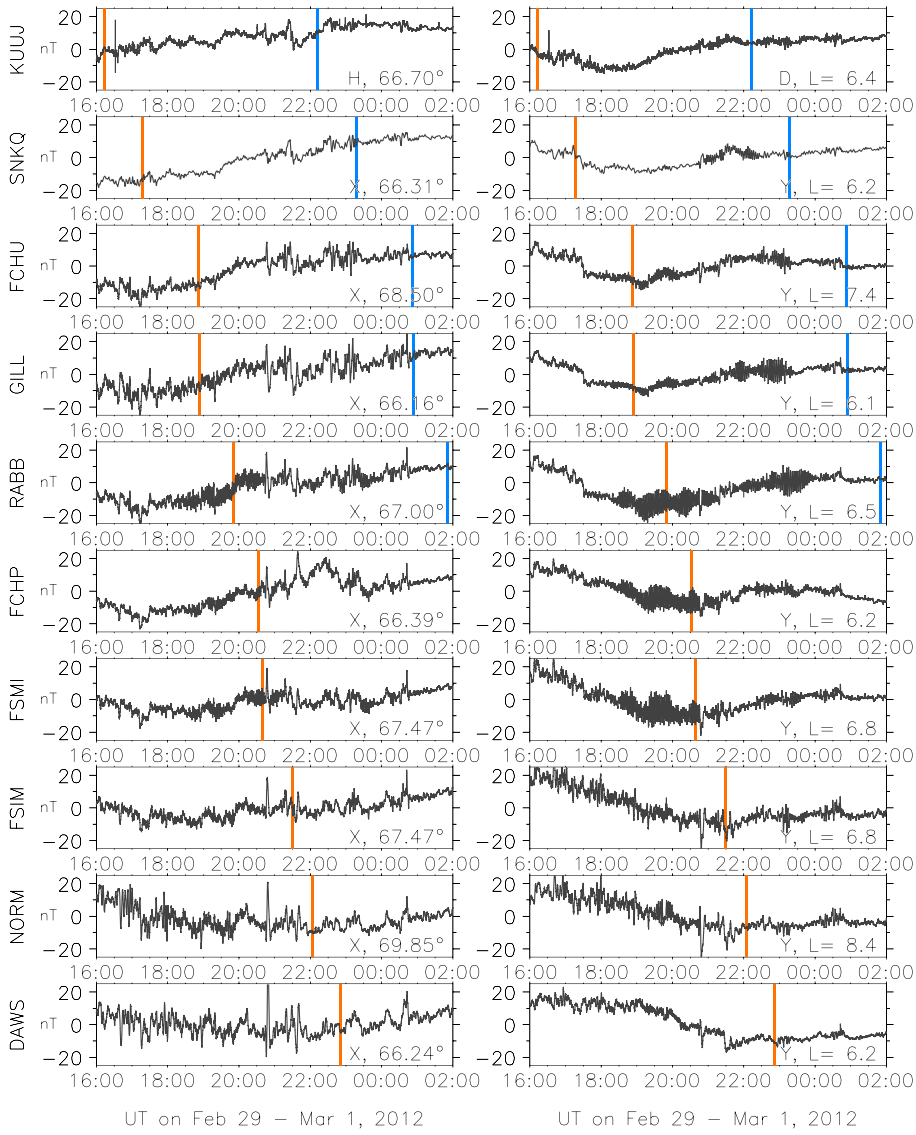

Figure 4. Horizontal (left column) northward and (right column) eastward components of the magnetic field at 10 selected stations. The orange and blue vertical lines indicate local magnetic noon (12h MLT) and dusk (18h MLT), respectively.

GOES13 (red) and GOES15 (green). When mapped to the ground along the T96 model magnetic field, GOES13 was close to SNKQ and GOES15 was close to FSIM.

Occurrence of a ground Pg at a given instance (in a 10min UT data window) is determined by the following criteria: (1) the *Y* power spectrum has a peak between 4 and 6mHz; (2) the peak is the highest in the entire band covered by the spectrum, from zero to the Nyquist frequency; and (3) at the frequency of the peak, the *Y* power is higher than the *X* power. For GOES, we apply the same criteria to B_v (in place of *Y*) and B_ϕ (in place of *X*) to define the occurrence of Pgs, noting that previous studies reported that Pgs are associated with poloidal mode waves in the magnetosphere [*Kokubun et al.*, 1989; *Takahashi et al.*, 2011]. The Pg activity occupies two domains in the UT-MLT space. One domain covers 0700–1330 MLT and 1800–2030 UT, and the other covers 1400–1800 MLT and 2000–2400 UT. In both domains, Pgs exhibit band-limited spectral enhancement at ~6mHz (period ~180s), but the afternoon spectral peaks are slightly broader.

3.3. Latitudinal and Longitudinal Variation of the Phase

We have examined the spatial phase variation of the Pg pulsations using the *Y* component data from GILL ($L = 6.15$, geomagnetic longitude = 333.05°) and two other stations with a small separation from GILL in either

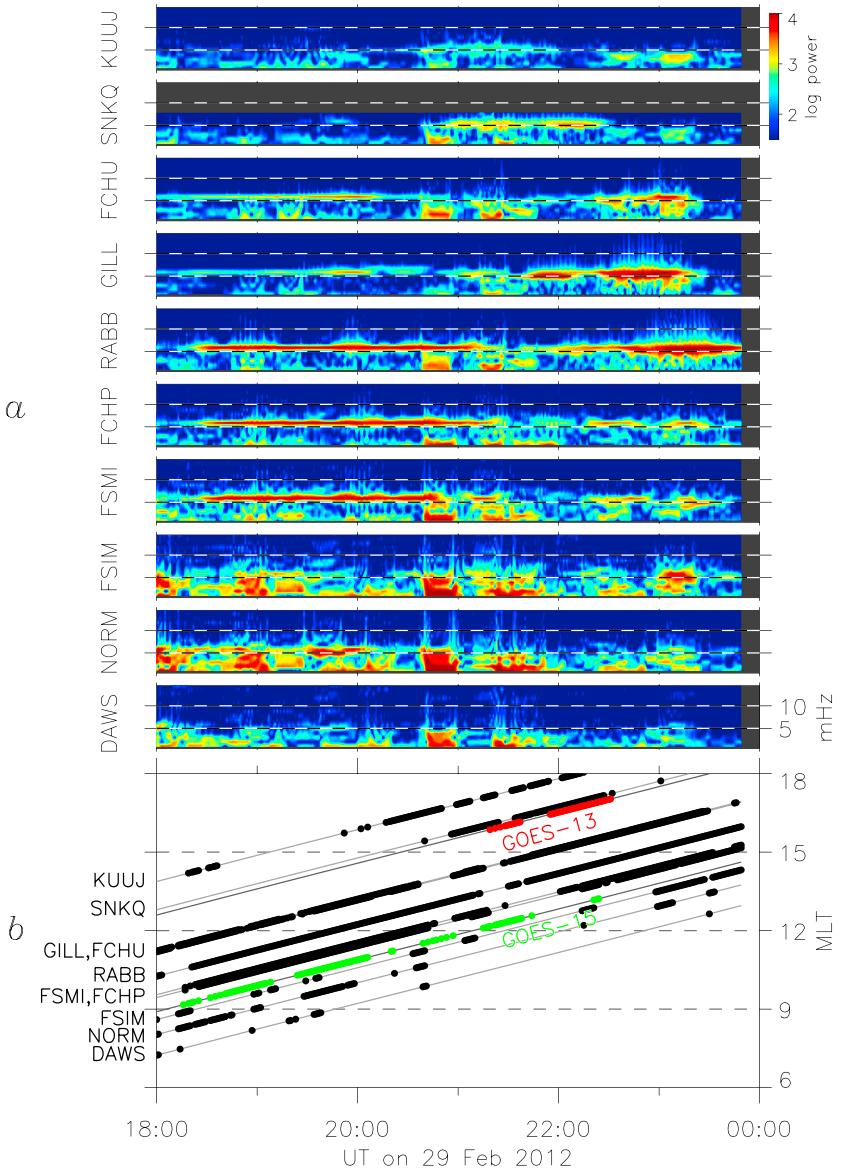

Figure 5. Summary of Pg activity on 29 February 2012. (a) Dynamic power spectra of the magnetic field eastward component at the 10 stations shown in Figure 4. (b) MLT of the Pg activity at the ground stations (black dots) and the poloidal mode activity at GOES13 (red dots) and GOES15 (green dots). Pg occurrence is judged in 10min steps.

longitude or latitude. We have selected the 2.5h interval 2115–2345 UT for analysis, and the results are shown in Figure 6. Figures 6a–6c show results from the three longitudinally separated stations, RABB (6.57, 311.91°), GILL, and SNKQ (6.45, 356.67°), and Figures 6d–6f show the results from the latitudinally separated stations, FCHU (7.44, 333.54°), GILL, and ISLL (5.15, 333.36°).

Figure 6a shows that Pgs are present at all three stations but that their amplitudes vary with UT differently. At SNKQ, the amplitude is large only in the first half of the time interval shown; at GILL, the amplitude is large in the middle (except for a minimum at 2210 UT); at RABB, the amplitude is larger in the second half. Overall, this gives us the impression that the region of Pg activity was moving westward or sunward.

We have applied a moving data window Fourier spectral analysis to the time series data plotted in Figure 6a and show the results in Figures 6b and 6c. The data window is 10min long, and it is shifted by 5min in successive steps. The power spectra averaged over 4–6mHz (Figure 6b) confirm the UT variation of the Pg amplitude described above.

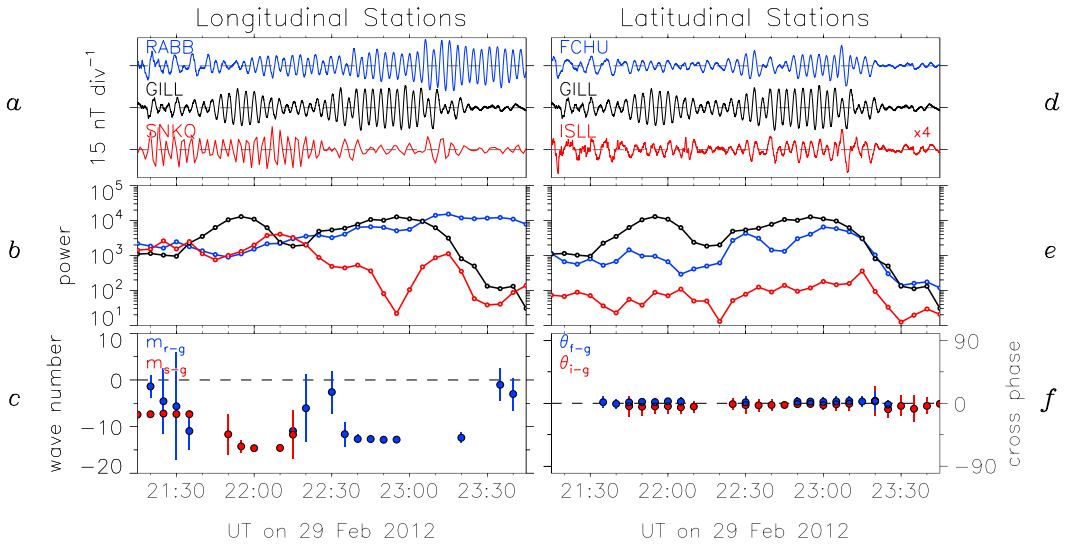

Figure 6. Comparison of the perturbations of the magnetic field *Y* component observed from 2115 to 2345 UT at stations close to each other. (a) High-pass-filtered *Y* components at the longitudinally separated stations RABB, GILL, and SNKQ. (b) Power spectral density of *Y* averaged from 4 to 6mHz. (c) Azimuthal wave number calculated from the RABB-GILL pair (blue) and SNKQ-GILL pair (red). The results are shown only at time steps with high coherence (>0.8) between the stations. The error bars indicate ± 1 standard deviation. (d) High-pass-filtered *Y* components at the three latitudinally separated stations, FCHU, GILL, and ISLL. Data from ISLL are shown with a magnified scale. (e) Power spectral density of *Y* averaged from 4 to 6mHz. (f) Cross phase between GILL and FCHU (blue) and between GILL and ISLL (red).

The azimuthal wave number m shown in Figure 6c is calculated using the phase delay ($\Delta\theta$, not shown) between the two pairs of stations, GILL-SNKQ (red) and GILL-RABB (blue). We use the relationship $m = \Delta\theta/\Delta\phi$ to determine m, where $\Delta\phi$ is the longitudinal separation of the stations. We assume that there is no $2n\pi$ ambiguity in the cross phase and define m to be positive for eastward propagation. All data points in Figure 6c are in the $m < 0$ domain, indicating that the waves propagated westward. The magnitude of m mostly lies between 10 and 15, except before 2140 UT when it is below 10. These results are consistent with previous observations except that the magnitude of our m is slightly smaller than those (16–35) reported previously [e.g., *Rostoker et al.*, 1979; *Glassmeier*, 1980; *Hillebrand et al.*, 1982; *Poulter et al.*, 1983].

We next examine the latitudinal phase variation (Figures 6d–6f). The figure format is the same in Figures 6d and 6e, while Figure 6f shows the cross phase instead of the azimuthal wave number. Figure 6d indicates that the envelope structure is similar between FCHU and GILL. The amplitude at ISLL is quite low, and its envelope structure cannot be seen clearly in the time series plot. However, Figure 6e shows that the temporal variation of the power at ISLL is similar to that at FCUH and GILL (when plotted in log scale). The cross phase (Figure 6f) is close to zero for either combination of the stations. The implication is that the pulsations were propagating westward maintaining a nearly constant phase over L ~5.0–7.5.

3.4. Spectral Properties of Pgs at GOES

We have both magnetic field and particle data from GOES to characterize Pg oscillations in space. In the previous geostationary satellite study of an afternoon Pg wave by *Thompson and Kivelson* [2001], only particle data were examined.

We first demonstrate that the Pgs originated from fundamental standing Alfvén waves. Figure 7 shows the 24h dynamic spectra of the three magnetic field components at GOES13. Four vertical dotted lines indicate reference local times to assist visual examination of the local time dependence of various wave modes.

Most spectral features seen on this day are similar to those reported previously at geostationary spacecraft [e.g., *Takahashi and McPherron*, 1984]. First, the azimuthal component exhibits several spectral peaks that originate from multiharmonic toroidal mode waves. The harmonic modes of these peaks are labeled T1 (fundamental mode) through T6 (sixth harmonic). The toroidal mode waves are present throughout most of the dayside portion of the orbit and have frequencies that fall with MLT due to increasing mass loading. Second, the radial component lacks a multiharmonic frequency structure but exhibits a strong peak at

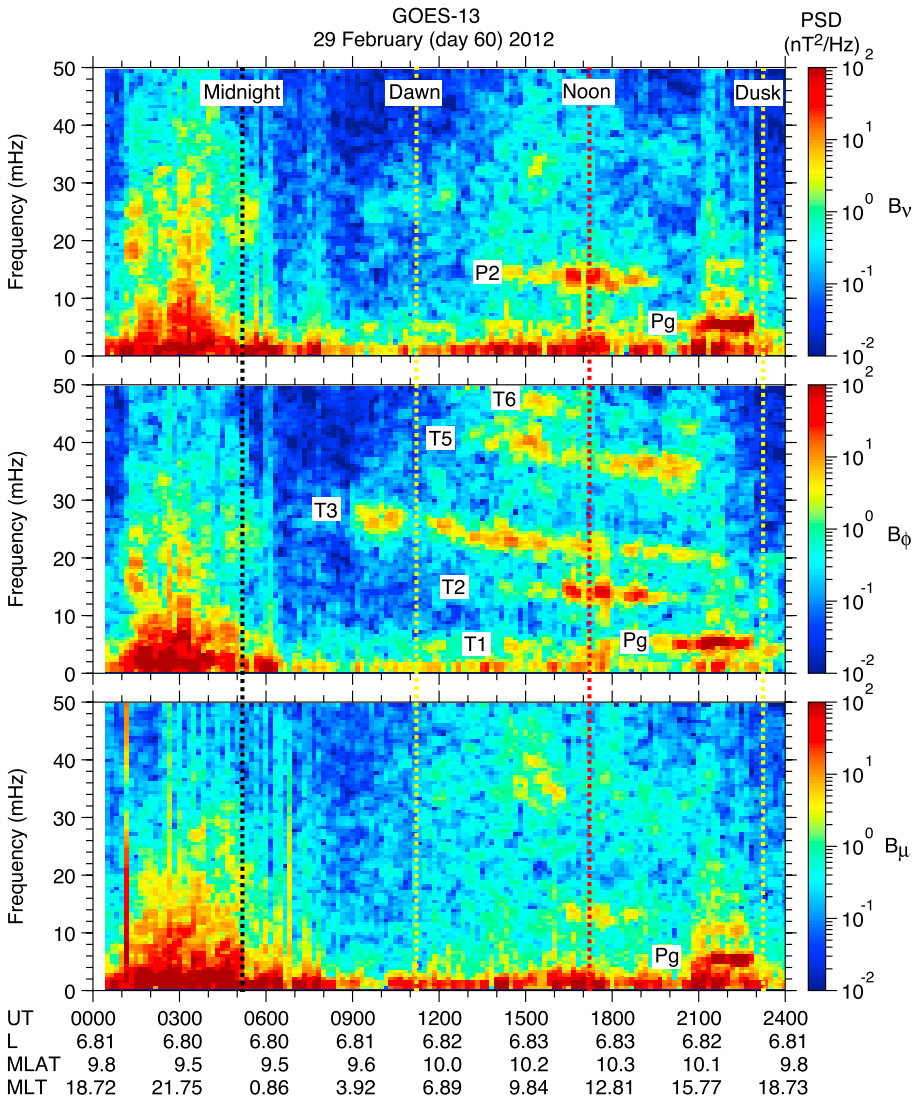

Figure 7. Full-day dynamic spectra of the magnetic field components at GOES13 for 29 February 2012. See section 3.4 for the explanation of the labeling of the prominent spectral peaks.

~15mHz around noon. This oscillation is identified to be the second harmonic poloidal mode wave (P2). This wave is likely excited by the bounce resonance mechanism [see *Liu et al.*, 2013, and references therein].

What is unique in Figure 7 is the strong peak (labeled "Pg") at ~5mHz (period ~ 200s) that appears near dusk in all three components, with higher spectral intensity in the poloidal (B_ν and B_μ) components than in the toroidal (B_ϕ) component. The Pg frequency at GOES matches that of the Pg observed on the ground near the footprint of this spacecraft (Figure 5). The Pg frequency is below the T2 and P2 frequencies but is close to the T1 frequency observed earlier. Based on these spectral features, we conclude that the Pg spectral peak originated from fundamental mode oscillation of field lines with a strong poloidal component. We will confirm later (in Figure 10) the correspondence between the Pg on the ground and the poloidal mode wave in space.

The ~5mHz magnetic field oscillations are accompanied by oscillations in particle fluxes. Figure 8 shows an overview of the SEM particle data from GOES13 for 1800–2400 UT on 29 February 2012. The left column shows the time series plots of the magnetic field (Figure 8a) and the proton and electron fluxes (Figure 8b). The shading indicates the time interval, 2130–2230 UT, of the strongest Pg signal at GOES13 recognized in Figure 7. Although oscillations in the particle fluxes are difficult to see in the compressed time and intensity scales of Figure 8b, the dynamic spectra shown in the right column indicate that the flux of both protons and electrons (Figure 8d) oscillates at the same frequency as the magnetic field (Figure 8c).

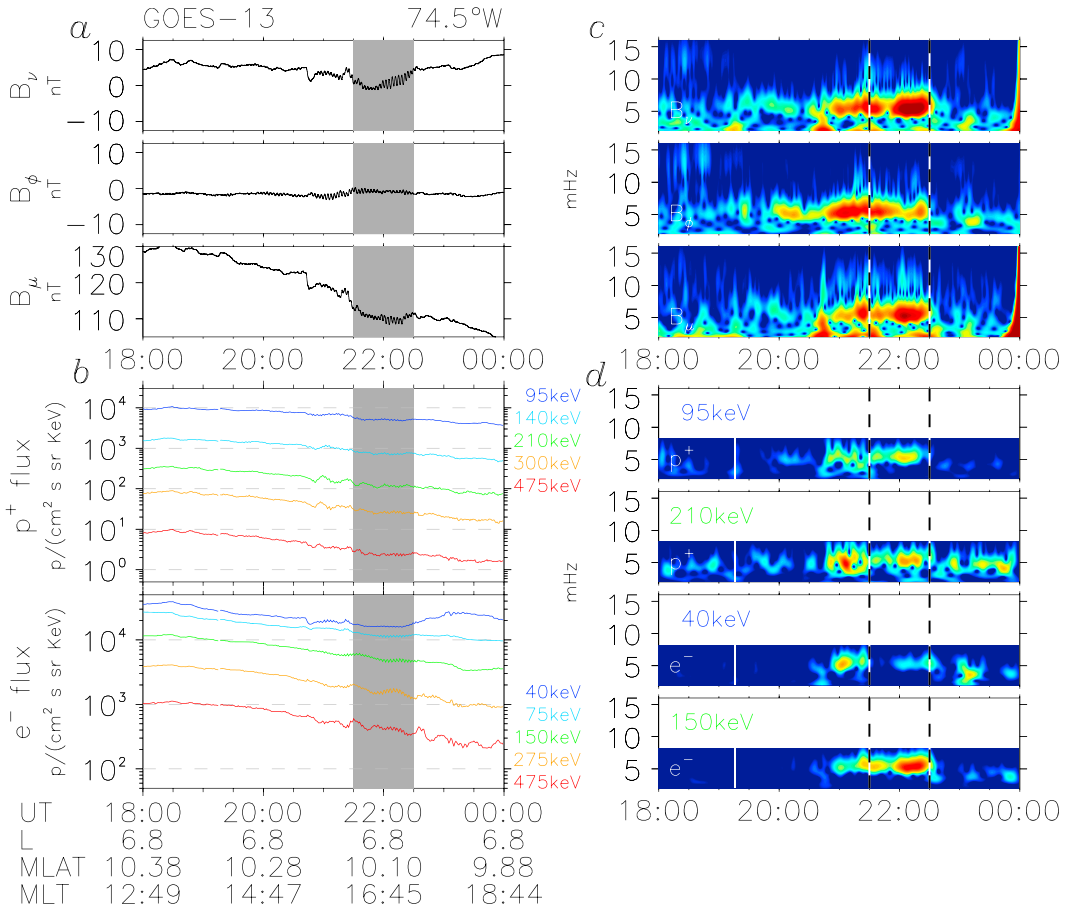

Figure 8. Overview of GOES13 measurements. (a) Three components of the magnetic field in the field-aligned coordinates. (b) Flux of protons and electrons. (c) Dynamic power spectra of the magnetic field. (d) Dynamic power spectra of proton (P1 and P3) and electron (E1 and E3) fluxes. The spectra were calculated using detrended flux values, obtained by subtracting the 5min running mean from the original data.

Figure 9 shows the same analysis done to the GOES15 data. At this spacecraft, oscillations corresponding to the ground Pg occurred at ~4–6mHz. Magnetic field signatures of these oscillations are present at 1830–2030 UT, but they are weak compared with GOES13. This difference is attributed to the different magnetic latitudes of the two spacecraft. GOES13 was located at magnetic latitude (MLAT) ~10°, while GOES15 was located at MLAT ~4°, meaning that the latter spacecraft was closer to the equatorial node of the B_ν component of a fundamental poloidal mode wave. Another distinct difference from GOES13 is seen in the energetic particle fluxes. During the intervals of the ground Pg activity at RABB (1830–2130 UT and 2230–2400 UT; see Figure 5b), strong oscillations occurred in the proton flux, at 210keV in particular, but oscillations are hardly visible in the electron flux (Figure 9d) unlike at GOES13. We examine the proton flux oscillation in more detail in section 3.5 for possible evidence of drift resonance. The electrons cannot be in drift resonance with the westward propagating wave. Therefore, the electron flux oscillations are likely caused by radial convection of a density gradient [*Southwood and Kivelson*, 1981; *Takahashi et al.*, 1985].

3.5. Energy Dependence of Particle Flux Oscillations at GOES

Following previous observational studies of particle drift resonance with a fundamental poloidal mode wave [*Thompson and Kivelson*, 2001; *Dai et al.*, 2013], we examine the energy dependence of ion flux oscillations during the Pg event. The expected signatures are an amplitude peak of flux oscillations at the energy of the resonance and a 180° phase shift across the resonance energy [e.g., *Southwood and Kivelson*, 1981], with oscillations at lower energies lagging behind oscillations at higher energies [*Dai et al.*, 2013]. At the resonance energy, the ion flux should oscillate in quadrature with B_ν [*Southwood and Kivelson*, 1981] and in phase with the azimuthal component of the electric field E_ϕ [*Dai et al.*, 2013]. The GOES spacecraft do not measure the electric field, but we infer from the standing wave mode structure of the fundamental poloidal mode that B_ν

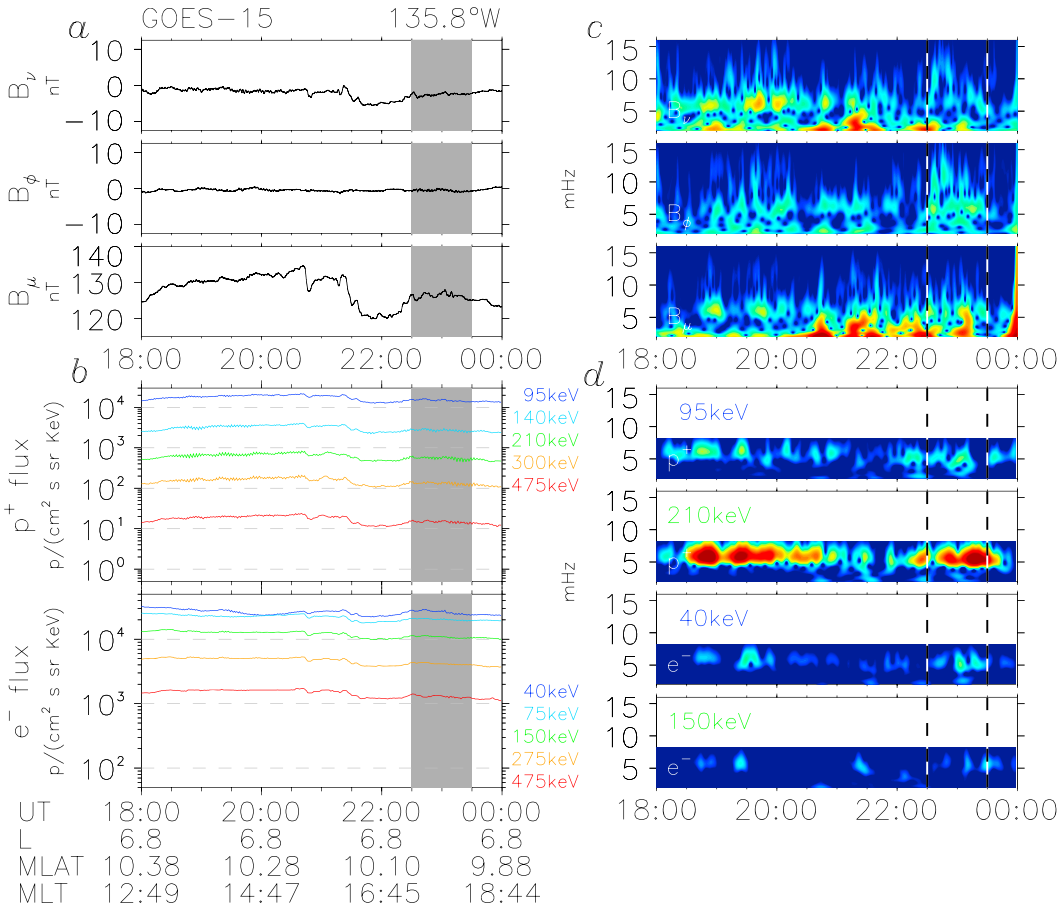

Figure 9. Overview of GOES15 measurements in the same format as Figure 8.

leads E_ϕ by 90° at the magnetic latitude of GOES13 [see *Takahashi et al.*2011, Figure 2a]. Thus, for the type of drift resonance reported by *Dai et al.* [2013], proton flux oscillation at the resonance energy should lag behind the B_ν oscillation by 90°. Finally, we can estimate the energy of protons in drift resonance with the observed poloidal wave based on the measured frequency (5mHz) and m number (−12, see Figure 6c) of the wave. Using the formula [*Hamlin et al.*, 1961] for the guiding center drift frequency of equatorial particles in a dipole magnetic field, we find that the resonance occurs at 160keV for the GOES15 L value of 6.8.

Figure 10a shows the details of the magnetic field and proton flux oscillations at GOES13 at 2130–2230 UT (1615–1715 MLT). The filtered ground Y components at SNKQ and GILL (first panel), which were near the footprint of the GOES13 satellite, are very similar to the filtered B_ν component at the spacecraft (second panel), providing convincing evidence that the spacecraft detected the source wave of the Pgs observed on the ground. The third panel shows normalized perturbations of the ion flux defined by $(J - J_{RM})/J_{RM}$, where J is the raw proton flux and J_{RM} is its 5min running mean. The fourth panel captures some features of proton flux oscillations displayed in the third panel, by displaying the power of proton flux oscillation at the frequency of the B_ν oscillations and at the proton energy that exhibits the highest power. The frequency of the B_ν oscillation and the proton flux oscillation power were evaluated in a moving 3min data window, and the color of the dots indicates the particular proton energy at the given time step. We find that protons with energy ≥210keV exhibit the highest power throughout the interval displayed. The fifth panel shows the cross phase between B_ν and proton flux at the five energies (using the same color code as in the time series plots.)

Flux oscillation that has the same period as the ground Pg and satellite B_ν oscillation is evident in each proton channel, indicating a causal relationship between the wave and the particle flux oscillations. Both the amplitude and phase of the flux oscillation are energy dependent, a possible signature of drift resonance. However, the proton flux oscillations do not provide information to confirm the resonance. Although the phase of flux oscillations at lower energy is delayed with respect to those at higher energies, in accordance with the event

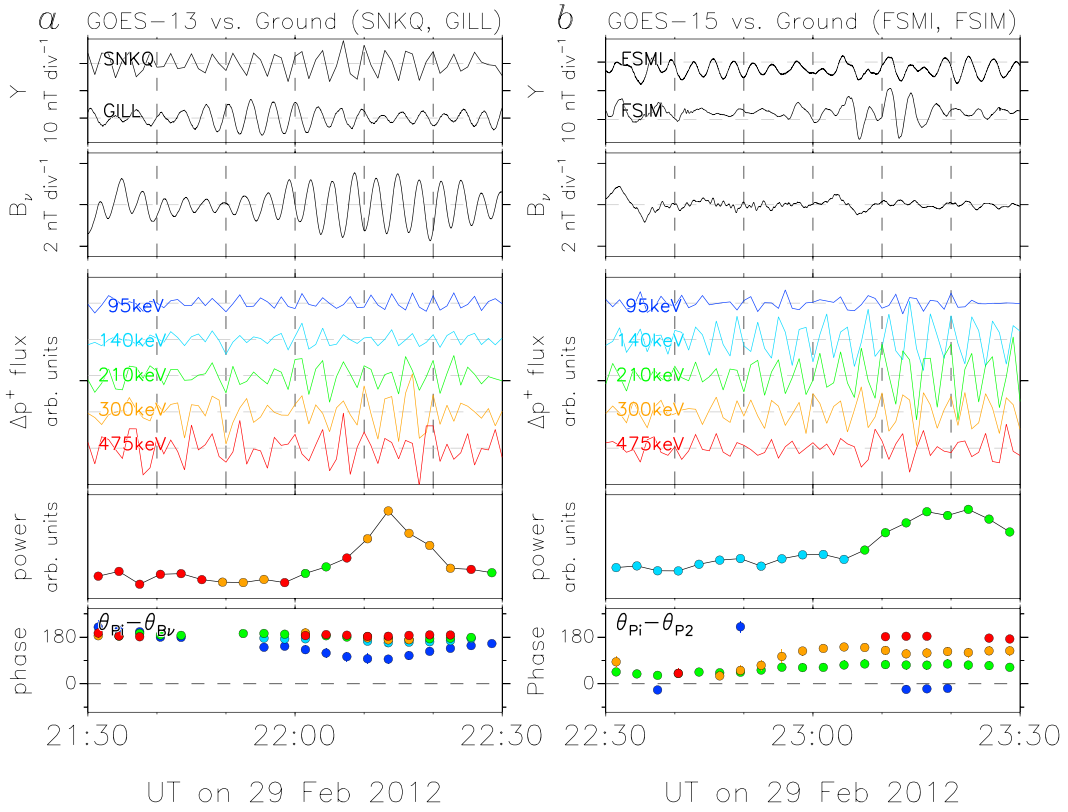

Figure 10. (a) Comparison of observations at 2130–2230 UT at GOES13 and two ground stations near the footprint of the satellite. (first panel) Ground magnetic field *Y* components; (second panel) the radial component (B_ν) of the magnetic field at the satellite; (third panel) normalized variation of the flux of protons at five energies; (fourth panel) the upper envelope of the power spectral density of the proton flux oscillations at the five energies; and (fifth panel) the cross phase between B_ν and the proton fluxes. (b) Comparison of observations at 2230–2330 UT at GOES15 and ground stations near the footprint of the satellite. The format is the same as Figure 10a except that the cross phase is calculated using the proton flux at 140keV as the reference.

reported by *Dai et al.* [2013], the phase shift is not significant at the energy (300keV) of the maximum amplitude. Also, around the predicted drift resonance energy of 160keV, the proton flux oscillates ~180° out of phase with B_ν, which does not match the theoretical prediction of a 90° phase difference [*Southwood and Kivelson*, 1981].

Figure 10b shows data from the FSMI and FSIM ground magnetometers and the GOES15 satellite for 2230–2330 UT (1310–1410 MLT at GOES15). At GOES15, there is no clear oscillation in B_ν that corresponds to the ground Pgs observed near the footprint of the spacecraft. As stated above, we believe that this is due to the proximity of the spacecraft to the B_ν node at the magnetic equator. Ion flux oscillations very similar to those observed at GOES13 are detected (third panel), which implies that the ions were responding to the E_ϕ component of the fundamental poloidal mode. The amplitude of E_ϕ must have been substantial because it has an antinode at the magnetic equator. The phase of ion flux oscillations is again energy dependent, as shown in the fifth panel. Unlike at GOES13, however, the phase shifts by ~180° over the five energy steps, as seen at ~2315 UT. This is possible evidence of drift resonance. However, we cannot conclude that drift resonance occurred in the same manner as in the case reported by *Dai et al.* [2013] because we do not have information on the **E** or **B** field oscillations.

4. Statistical Analysis of Ground Pgs

The unusual local time extent of the 29 February 2012 event motivated us to examine ground magnetometer data for a statistical evaluation of the properties of Pgs on the afternoonside. From a survey of data covering 2008–2013, we find that afternoon Pgs did occur at a rate much higher than that expected from the statistics presented by *Brekke et al.* [1987] (see Figure 1).

4.1. Method of Event Identification

We have identified Pg events through visual inspection of magnetometer data from the stations in North America that are described in section 2 and listed in Table 2. The stations cover an *L* range of 3.8–7.4. Pgs usually occur during geomagnetically quiet periods, and the strikingly regular waveforms of Pgs are easy to spot in magnetic field time series plots. Our criteria for a Pg event at a given station are as follows: (1) the horizontal components (*H* and *D*, or *X* and *Y*, depending on the station) exhibit a monochromatic oscillation in the period range of 20–200s and (2) the amplitude is larger in the eastward (*Y* or *D*) component than in the northward (*H* or *X*) component.

For each Pg event at a given station, we determined its start UT, its end UT, and its frequency and entered these parameters into a Pg event list along with the position information for the station. If a Pg is detected at multiple stations, information is registered separately for all the stations. The *H* (or *Y*) amplitude of the selected Pgs is in the range 2–20nT, and the duration of an event at an individual station is in the range 8–210min. We have identified a total of 105 events by counting events detected at multiple stations at a given UT as separate events. Some events occurred simultaneously at up to three stations.

Also included in the list are the solar wind velocity and geomagnetic activity indices (*Dst* and *AL*). We have chosen the *AL* index value that is the minimum in the 5h interval preceding the onset of a Pg. The idea behind this choice is that it takes a finite amount of time for particles responsible for Pg waves to arrive at the point of observation after they are injected from the midnight sector at the onset of a substorm.

4.2. Spatial Distribution of Pg Events

Figure 11a shows the *L*-MLT map of the 105 Pg events. Each event is marked by an arc, which is color coded according to the period of the pulsation. The radial distance of the arc indicates the *L* value of the station, the azimuthal span of the arc indicates the MLT span of the event, and the dot indicates the center of the event. Black dots are added to the events observed on 29 February 2012. Most events occurred in the *L* range 5–7, with a few events occurring at $L \sim 4$ and at $L \sim 7.4$. Pgs are known to occur most often at the auroral latitude ($L = 6$–7), but Pgs at nominal plasmaspheric latitudes ($L < 4$) [*Green*, 1985] are not unheard of. Therefore, the *L* distribution of our events provides no great surprise. However, the MLT distribution is a different story. We find Pgs in the postnoon sector, including the one observed on 29 February 2012.

Figure 11b shows the MLT distribution of the events. The light gray histogram was generated by allowing for multiple counts of an event at a given UT at different stations. The UT of the events is converted to MLT in 10min steps and is accumulated in the hourly MLT bins. The dark gray histogram (morning) and green histogram (afternoon) were generated by eliminating duplicate counts of an event occurring at the same UT. In either histogram, it is clear that Pgs occur on the afternoonside at a surprisingly high rate in comparison to the historical result shown in Figure 1.

4.3. MLT Dependence of Pg Period

Having found Pgs on the afternoonside, we ask the question of whether the newly found afternoon Pg population is different from the well-known Pgs detected on the morningside. For the Pg event on 29 February 2012, we showed that the pulsation originated from a fundamental poloidal mode wave. Because the period of the poloidal mode wave depends on the mass density and magnetic field like any other standing Alfvén waves, we expect the Pg period to depend on MLT as the period of the fundamental toroidal mode (T1) waves does, if Pgs originate from the fundamental poloidal mode wave regardless of local time. As inferred from the multiharmonic toroidal mode waves shown in Figure 7 and in many geostationary observations [e.g., *Junginger et al.*, 1984], the T1 period increases from morning to afternoon owing to the increase of the plasma mass density [e.g., *Takahashi and McPherron*, 1984]. Because the period of standing Alfvén waves depends on *L* as well, we need to consider both the MLT and *L* dependence Pg period in relating the pulsations to a particular standing wave harmonic.

Figure 12a shows the MLT dependence of the *L* and period of the Pgs in our event list. The *L* shells of the events are mostly in the range 5–7, confirming previous observations [e.g., *Chisham and Orr*, 1991]. The *L* value exhibits an upward trend in the postmidnight sector (00–06h MLT) and a large scatter in the prenoon sector (06–12h MLT). The *L* value in the afternoon is on average higher than in the morning. The event on 29 February occurred at higher *L*s than the average.

Figure 12b shows the average Pg period (solid red circles) calculated by limiting to Pgs observed at a narrow range of $5.5 < L < 6.5$ to eliminate the *L* dependence of the period. The period shows an increase from ~80s

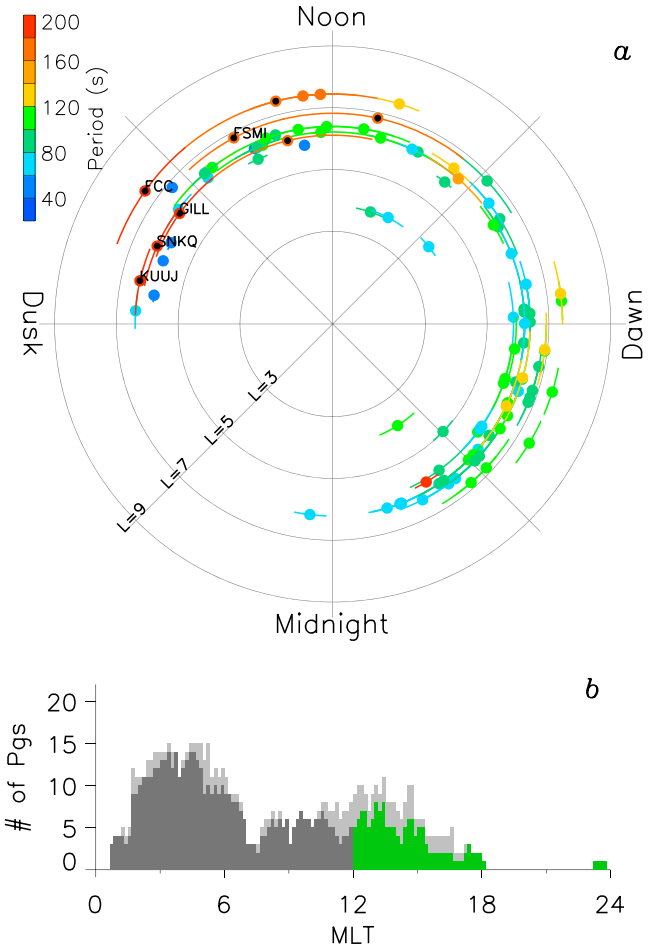

Figure 11. (a) MLT-*L* distribution of the 103 Pg events detected in 2008–2013. See section 4.2 for explanation. (b) Distribution of Pgs as a function of MLT. See section 4.2 for the histograms in different colors.

(frequency ~13mHz) at 00–03h MLT to ~140 s (~7mHz) at 15–18h MLT. According to a statistical study of spacecraft magnetometer data [*Takahashi and Anderson*, 1992], the average T1 frequency at $L = 6.0$ is ~10mHz (period ~100s) for 09–12h MLT. This is in good agreement with the average period of our Pg events in the same MLT sector and provides convincing evidence that Pgs originate from fundamental mode oscillations of the geomagnetic field line. The 29 February 2012 event (blue dots) had a period longer than the averages, which can be attributed to the fact that the event was excited at higher *L*s than average.

4.4. Comparison of Morning and Afternoon Events

We have compared some statistical properties of morning and afternoon Pgs. Figure 13a shows the distribution of the event duration. The duration of the afternoon Pgs is shorter, with most events lasting <1h. The afternoon Pg event on 29 February 2012 is an exception. By contrast, Pgs had a duration >1h on many mornings.

Figure 13b shows the seasonal variation of the occurrence. The morning events occur in all seasons, with a minimum in the winter months of December and January. There is no summertime minimum, which is very different from the seasonal pattern reported by *Brekke et al.* [1987]. The afternoon events, by contrast, are absent during the summer.

Figures 14a–14c present the solar wind velocity and geomagnetic indices distribution of morning and afternoon Pgs. Here the *Dst* (*AL*) index was used as an indicator of a geomagnetic storm (substorm). As reported in previous studies, most of our Pgs occurred at times of low solar wind velocities and low geomagnetic activities. The only notable difference is that the afternoon Pgs are associated with higher solar wind

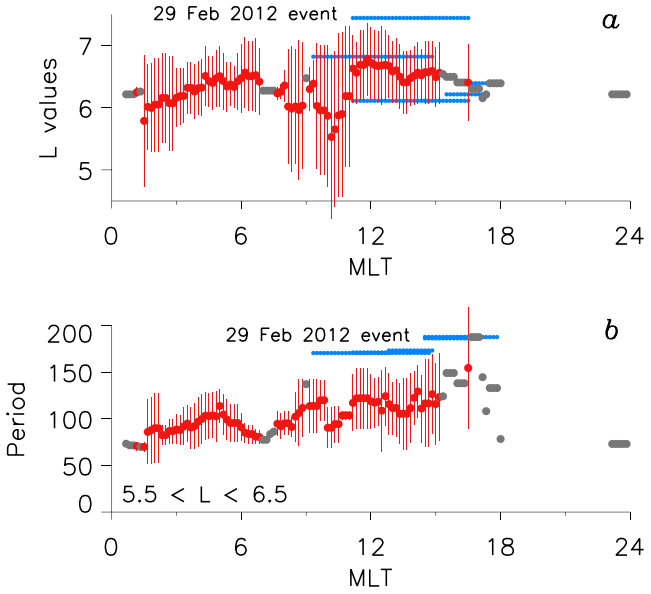

Figure 12. (a) MLT dependence of the *L* value of the stations that detected Pgs. Pg events are placed into 10min MLT bins for this figure. The red and gray filled circles are the averages in the MLT bins. The red error bars are the standard deviations, shown for MLT bins containing more than five samples. The blue dots indicate the *L* value of the individual stations that detected Pgs on 29 February 2012. (b) MLT dependence of the period of Pgs. The red and gray filled circles are averages calculated for events detected at $L = 5.5–6.5$. The vertical bars are the standard deviations. The blue dots indicate the observed periods of the Pg event on 29 February 2012.

velocity (Figure 14a). However, the higher velocity does not translate to higher substorm activity because we do not see any obvious difference in the distribution of minimum *AL* between morning and afternoon Pgs (Figure 14c).

The *AL* distributions shown in Figure 14c are consistent with the finding by *Rostoker at al.* [1979] that Pgs occur as the magnetosphere recovers from previous activities (substorms). This figure shows that the *AL* value has the highest occurrence in the 0 to −50nT bin and that the occurrence is significantly lower in the bins covering −50 to −350nT. In contrast, the Pg occurrence rate is not peaked in the 0 to −50nT *AL* bin. This means that most Pgs are associated with a weak or moderate auroral electrojet activity in the preceding 5h, which may

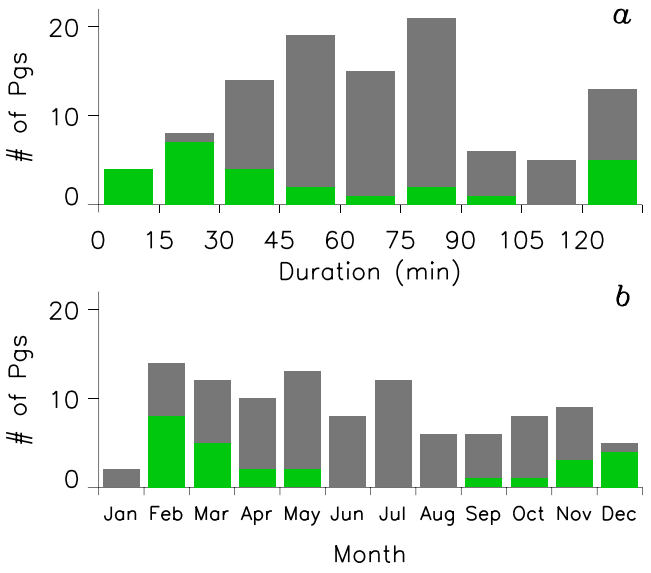

Figure 13. (a) Distribution of the duration of Pgs. The bars are color coded according to the MLT of observation: gray for morning and green for afternoon. (b) Seasonal distribution of Pg. The color coding is the same as in Figure 13a.

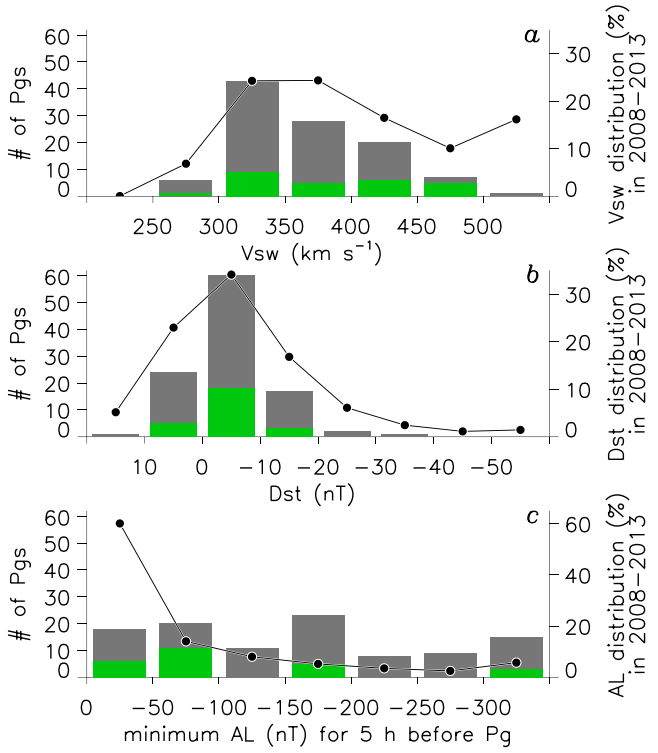

Figure 14. Distributions of Pg occurrence as a function of (a) solar wind speed, (b) *Dst* index, and (c) *AL* index. The bars are color coded according to the MLT of observation: gray for morning and green for afternoon. The distribution (%) of Vsw, *Dst*, and *AL* for the whole of 2008–2013 is also presented.

correspond to the period of substorm recovery. This result is reasonable because it is very likely that energetic ions injected into the inner magnetosphere from the magnetotail provide energy to Pgs.

We also examined whether Pgs occurred during the recovery phase of geomagnetic storms. Following *Dai et al.* [2015], who studied the *Dst* dependence of poloidal Pc4 waves observed by spacecraft, we defined late storm recovery phase as the period during which the *Dst* value changes from 50% of its minimum to zero. Of the 105 Pg events, 34 (including the 29 February 2012 event) occurred in the late recovery phase of a geomagnetic storm, where we required the *Dst* minimum to be lower than −20nT for storms. The remaining 71 events (70% of all events) occurred during geomagnetically quiet periods that cannot be classified into any phase of a geomagnetic storm. This result suggests that the recovery phase of a geomagnetic storm is not a strong requirement for Pg generation. *Dai et al.* [2015] found that poloidal Pc4 waves occur preferentially during the recovery phase, which is not surprising because most of their events had the signature of a second harmonic standing Alfvén wave, and the wave is unlikely to produce a Pg event on the ground [*Takahashi et al.*, 1992]. Occurrence of Pgs during nonstorm periods means that the presence of a storm time ring current is not a requirement for the excitation of the pulsations.

5. Discussion: Comparison With Previous Results

Our study detected a large number of afternoon Pgs, unlike previous studies. There are two possible reasons for the difference. One is the methodology. The study by *Brekke et al.* [1987], which we consider to be a benchmark for its coverage of multiple solar cycles, relied on analog records from a single station located at L~6.3. By contrast, we used digital data from multiple stations covering $L = 3.8–7.4$. The quality and spatial coverage of the data are obviously better in our study, allowing for detection of events with lower amplitudes and over a wide range of latitudes. Our afternoon Pgs had short durations except for the event selected for a case study. Such short-duration events could have been missed in the visual survey of the analog records. In addition, we note that our afternoon events are detected at higher L than the morning Pgs (Figure 12a). It is possible that for the time period covered by the *Brekke et al.* [1987] study, there were many afternoon Pgs that occurred at latitudes higher than Tromsø.

The other possibility is that the solar and geomagnetic conditions for our survey, 2008–2013, were very quiet. The monthly sunspot number (provided by the Solar Influence Data Center, http://sidc.oma.be) averaged over the period 1929–1985 covered by *Brekke et al.* [1987] is 69.8, while the average over 2008–2013 is 33.4. The low solar (and correspondingly low geomagnetic) activity during the period for our event survey may have changed the ring current intensity and location as well as the location of the plasmapause and plasma mass density from those under average geomagnetic conditions so that the ring current instability responsible for Pgs occurred even on the afternoonside. Future studies of Pgs should address how the occurrence of drift resonance or another mechanism for excitation of the fundamental poloidal mode is controlled by the geomagnetic activity. Such studies may include modeling of ring current development with realistic boundary conditions to address how the phase space density favorable for the poloidal mode excitation develops.

6. Conclusions

In conclusion, we have studied the local time dependence of the occurrence and physical properties of Pgs using data from geostationary satellites and ground magnetometers. We examined in detail an event in February 2012, which was observed from ~08 to ~18h MLT and exhibited periods >150s, exceeding the typical Pg period of ~100s. For this event we confirmed that the pulsation was associated with a fundamental poloidal mode wave observed by GOES geostationary spacecraft. Furthermore, the period of ground Pgs identified in the present study increased from morning to afternoon similar to that of fundamental toroidal mode waves reported previously at geostationary orbit [e.g., *Junginger et al.*, 1984]. Because the theoretical fundamental poloidal and toroidal mode periods are typically within 30% of each other [*Cummings et al.*, 1969] and previous ground-satellite conjugate observations on the morningside identified fundamental poloidal mode waves as the Pg source [e.g., *Takahashi et al.*, 2011], this similarity suggests that Pgs originate from fundamental poloidal mode waves at all local times. Again, it is also worth noting that whereas 34 (including the 29 February 2012 event) of all the 105 Pg events occurred in the late recovery phase of a geomagnetic storm, the remaining 71 events occurred during nonstorm periods. This result provides insight into the Pg generation mechanism; i.e., the presence of a storm time ring current is not a strong requirement for Pg generation. The frequent occurrence of afternoon Pgs in our survey, compared to previous ones, *Brekke et al.* [1987] in particular, might be caused by the difference in the data set and event selection methods. It is also possible that the solar activity level controls the local time distribution of Pgs. The period for our event survey, 2008–2013, is known for unusually low geomagnetic activity. At this time, we have no scenario of how this condition can cause Pgs to expand to later local time.

Acknowledgments

Work was supported by NASA grants NNX10AK93G, NNX13AE02G, and NNX14AB97G. The GOES magnetic field and energetic particle data are publicly available from NOAA National Centers for Environmental Information (formerly the National Geophysical Data Center). The ground magnetometer data are publicly available from the following magnetometer arrays: THEMIS GBOs (Principal Investigators (PIs): S. Mende and C.T. Russell), CARISMA (PI: I. Mann), CANMOS (PI: D. Calp), USGS (PI: C.A. Finn), and University of Alaska (PI: D. Hampton). We are grateful to the magnetometer PIs and team members for operating/maintaining the instruments as well as for making the data publicly available. We also acknowledge NASA contract NAS5-02099 and V. Angelopoulos for use of data from the THEMIS Mission, specifically GBOs. CARISMA is operated by the University of Alberta and funded by the Canadian Space Agency. CANMOS is operated by the Geological Survey of Canada.

Larry Kepko thanks Mark Engebretson and another reviewer for their assistance in evaluating this paper.

References

Birkeland, K. (1901), Expédition Norvégienne de 1899?1990 pour l'étude des aurores boréalres. Résultats des recherches magnétiques, *Videnskabsselsk. Skr, I. Mat. Naturvidensk. K.*, *1*, 1–80.

Brekke, A., T. Feder, and S. Berger (1987), Pc4 giant pulsations recorded in Tromsø, 1929–1985, *J. Atmos. Terr. Phys.*, *49*(10), 1027–1032.

Chen, L., and A. Hasegawa (1991), Kinetic theory of geomagnetic pulsations: 1. Internal excitation by energetic particles, *J. Geophys. Res.*, *96*(A2), 1503–1512.

Chisham, G. (1996), Giant pulsations: An explanation for their rarity and occurrence during geomagnetically quiet times, *J. Geophys. Res.*, *101*(A11), 24,755–24,763.

Chisham, G., and D. Orr (1991), Statistical studies of giant pulsations (Pgs): Harmonic mode, *Planet. Space Sci.*, *39*(7), 999–1006.

Cummings, W. D., R. J. O'Sullivan, and P. J. Coleman Jr. (1969), Standing Alfvén waves in the magnetosphere, *J. Geophys. Res.*, *74*(3), 778–793.

Dai, L., et al. (2013), Excitation of poloidal standing Alfvén waves through drift resonance wave-particle interaction, *Geophys. Res. Lett.*, *40*, 4127–4132, doi:10.1002/grl.50800.

Dai, L., et al. (2015), Storm time occurrence and spatial distribution of Pc4 poloidal ULF waves in the inner magnetosphere: A Van Allen Probes statistical study, *J. Geophys. Res. Space Physics*, *120*, 4748–4762, doi:10.1002/2015JA021134.

Glassmeier, K.-H. (1980), Magnetometer array observations of a giant pulsation event, *J. Geophys. Res.*, *48*, 127–138.

Glassmeier, K. H., S. Buchert, U. Motschmann, A. Korth, and A. Pederson (1999), Concerning the generation of geomagnetic giant pulsations by drift-bounce resonance ring current instabilities, *Ann. Geophys.*, *17*, 338–350.

Green, C. A. (1979), Observations of Pg pulsations in the Northern Auroral zone and at lower latitude conjugate regions, *Planet. Space Sci.*, *27*, 63–77, doi:10.1016/0032-0633(79)90148-X.

Green, C. A. (1985), Giant pulsations in the plasmasphere, *Planet. Space Sci.*, *33*(10), 1155–1168, doi:10.1016/0032-0633(85)90073-X.

Hamlin, D. A., R. Karplus, R. C. Vik, and K. M. Watson (1961), Mirror and azimuthal drift frequencies for geomagnetically trapped particles, *J. Geophys. Res.*, *66*(1), 1–4.

Hillebrand, O., J. Mnch, and R. K. McPherron (1982), Ground-satellite correlative study of a giant pulsation event, *J. Geophys. Res.*, *51*, 129–140.

Junginger, H., G. Geiger, G. Haerendel, F. Melzner, E. Amata, and B. Higel (1984), A statistical study of dayside magnetospheric electric field fluctuations with periods between 150 and 600 s, *J. Geophys. Res.*, *89*(A7), 5495–5505.

Kokubun, S. (1980), Observations of Pc pulsations in the magnetosphere: Satellite-ground correlation, *J. Geomagn. Geoelectr.*, *32*(SII), 17–39.

Kokubun, S., K. N. Erickson, T. A. Fritz, and R. L. McPherron (1989), Local time asymmetry of Pc 4–5 pulsations and associated particle modulations at synchronous orbit, *J. Geophys. Res.*, *94*(A6), 6607–6625.

Liu, W., J. B. Cao, X. Li, T. E. Sarris, Q.-G. Zong, M. Hartinger, K. Takahashi, H. Zhang, Q. Q. Shi, and V. Angelopoulos (2013), Poloidal ULF wave observed in the plasmasphere boundary layer, *J. Geophys. Res. Space Physics*, *118*, 4298–4307, doi:10.1002/jgra.50427.

Mann, I. R., et al. (2008), The upgraded CARISMA magnetometer array in the THEMIS era, *Space Sci. Rev.*, *141*, 413–451, doi:10.1007/s11214-008-9457-6.

Mende, S., et al. (2008), The THEMIS array of ground based observatories for the study of auroral substorms, *Space Sci. Rev.*, *141*, 357–387, doi:10.1007/s11214-008-9380-x.

Poulter, E. M., W. Allan, E. Nielsen, and K.-H. Glassmeier (1983), STARE radar observations of a Pg pulsation, *J. Geophys. Res.*, *88*, 5668–5676, doi:10.1029/JA088iA07p05668.

Rostoker, G., H. L. Lam, and J. V. Olson (1979), PC4 giant pulsations in the morning sector, *J. Geophys. Res.*, *84*(A9), 5153–5166.

Russell, C. T., et al. (2008), THEMIS ground-based magnetometers, *Space Sci. Rev.*, *141*, 389–412, doi:10.1007/s11214-008-9337-0.

Singer, H. J., L. Matheson, R. Grubb, A. Newman, and S. D. Bouwer (1996), Monitoring space weather with the GOES magnetometers, *Proc. SPIE Int. Soc. Opt. Eng.*, *2812*, 299–308.

Southwood, D. J. (1976), A general approach to low-frequency instability in the ring current plasma, *J. Geophys. Res.*, *81*(19), 3340–3348.

Southwood, D. J., and M. G. Kivelson (1981), Charged particle behavior in low-frequency geomagnetic pulsations: 1. Transverse waves, *J. Geophys. Res.*, *87*(A7), 5643–5655, doi:10.1029/JA086iA07p05643.

Takahashi, K., and B. J. Anderson (1992), Distribution of ULF energy ($f < 80$ mHz) in the inner magnetosphere: A statistical analysis of AMPTE CCE magnetic field data, *J. Geophys. Res.*, *97*(A7), 10,751–10,773.

Takahashi, K., and R. L. McPherron (1984), Standing hydromagnetic oscillations in the magnetosphere, *Planet. Space Sci.*, *32*, 1343–1359.

Takahashi, K., P. R. Higbie, and D. N. Baker (1985), Energetic electron flux pulsations observed at geostationary orbit: Relation to magnetic pulsations, *J. Geophys. Res.*, *90*, 8308–8318.

Takahashi, K., N. Sato, J. Warnecke, H. Luhr, H. E. Spence, and Y. Tonegawa (1992), On the standing wave mode of giant pulsations, *J. Geophys. Res.*, *97*(A7), 10,717–10,732.

Takahashi, K., R. E. Denton, and H. J. Singer (2010), Solar cycle variation of geosynchronous plasma mass density derived from the frequency of standing Alfvén waves, *J. Geophys. Res.*, *115*, A07207, doi:10.1029/2009JA015243.

Takahashi, K., K.-H. Glassmeier, V. Angelopoulos, J. Bonnell, Y. Nishimura, H. J. Singer, and C. T. Russell (2011), Multisatellite observations of a giant pulsation event, *J. Geophys. Res.*, *116*, A11223, doi:10.1029/2011JA016955.

Thompson, S. M., and M. G. Kivelson (2001), New evidence for the origin of giant pulsations, *J. Geophys. Res.*, *106*(A10), 21,237–21,253.

Tsyganenko, N. A. (1989), A magnetospheric magnetic field model with a warped tail current sheet, *Planet. Space Sci.*, *37*, 5–20.

Tsyganenko, N. A. (1995), Modeling the Earth's magnetospheric magnetic field confined within a realistic magnetopause, *J. Geophys. Res.*, *100*, 5599–5612.